A shallow approximation for ice streams sliding over strong beds

Katarzyna L. P. Warburton[1,4] (iD), Duncan R. Hewitt[2], Colin R. Meyer[1] and Jerome A. Neufeld[3,4,5]

[1]Thayer School of Engineering, Dartmouth College, Hanover, NH, USA; [2]Department of Mathematics, University College London, London, UK; [3]Department of Earth Sciences, University of Cambridge, Cambridge, UK; [4]Department of Applied Mathematics and Theoretical Physics, University of Cambridge, Cambridge, UK and [5]Institute for Energy and Environmental Flows, University of Cambridge, Cambridge, UK

Abstract

Ice streams are regions of rapid ice sheet flow characterised by a high degree of sliding over a deforming bed. The shallow shelf approximation (SSA) provides a convenient way to obtain closed-form approximations of the velocity and flux in a rapidly sliding ice stream when the basal drag is much less than the driving stress. However, the validity of the SSA approximation breaks down when the magnitude of the basal drag increases. Here we find a more accurate expression for the velocity and flux in this transitional regime before vertical deformation fully dominates, in agreement with numerical results. The closed-form expressions we derive can be incorporated into wider modelling efforts to yield a better characterisation of ice stream dynamics, and inform the use of the SSA in large-scale simulations.

1. Introduction

Numerical simulations of the flow of shear-thinning ice over the complex topography of ice-sheet beds using 3-dimensional full-Stokes models are computationally expensive, but in a wide variety of scenarios the geometry of the situation allows for simplified calculations to capture the dynamics (Hindmarsh, 2004). Ice is often much shallower than the horizontal scales on which driving stresses and average basal conditions vary, motivating shallow approximations where pressure gradients are hydrostatic (Cuffey and Paterson, 2010; Fowler, 2011). If the ice is frozen to the bed and vertical shear dominates the deformation, the shallow ice approximation (SIA) accurately captures the dynamics (Raymond, 1996). In fast-flowing regions of ice sheets where basal resistance is low, the dominant stresses are a combination of extensional stress and lateral shear, so the shallow shelf approximation (SSA) or depth-integrated membrane models provide lower-dimensional formulations (Morland, 1987; MacAyeal, 1989; Blatter, 1995; Pattyn, 2003; Hindmarsh, 2004; Schoof and Hindmarsh, 2010).

In simple geometries, such as wide, uniform ice streams, a further advantage of the SIA and SSA models is that they can be solved exactly to give closed-form expressions for the ice velocity and flux (Raymond, 1996). These expressions can then be used as a simple, essentially 1D representation of ice dynamics in models of related dynamical processes, such as the response of tidewater glaciers to calving (Benn and others, 2007), the impact of basal melt during Heinrich events (Mann and others, 2021) or interactions of the ice with its bed at the start of surges (Minchew and Meyer, 2020). However, the simplified expressions for the velocity and flux of ice have often been used beyond the regimes in which they are asymptotically valid, in particular in the transition from SSA to SIA as basal drag increases. Simply summing the two expressions (e.g. Mann and others, 2021) as an ad-hoc transition does not correctly capture the particular dynamics occurring in this rapidly sliding, high basal shear regime, as we show numerically and mathematically in this work. Furthermore, by understanding the transition between these flow regimes, the detailed flow profiles may be used to infer basal properties.

Small amounts of basal drag, such as would be experienced by an ice stream sliding over a bed of yielding sediment, can be viewed as a perturbation to the SSA expression for freely sliding flow. A natural question is at what point the flow becomes significantly modified, and whether this happens before reaching the fully non-sliding regime. Schoof and Hindmarsh (2010) mathematically examined the effect of basal drag as a higher-order correction to purely extensional flow. Here, motivated by the geometry of ice streams and their importance in wider models of ice sheet and climate dynamics, we look instead at the case where the dominant resistance to flow comes from lateral shear at the sidewalls, and the rheology of the shear margins is the primary control on the velocity of the stream (Meyer and Minchew, 2018; Hunter and others, 2021).

Since ice is shear-thinning, basal drag impacts not just the overall force balance but also the depth-averaged rheology. This motivates the 'L1L2' modelling framework (Hindmarsh, 2004) in which a linear approximation to the vertical shear acts to modify the ice viscosity. This framework has been implemented in large-scale ice-sheet models, including BISICLES, to capture ice flow dynamics lying between the SSA and SIA regimes (e.g. Goldberg and Sergienko,

2011; Cornford and others, 2013). The hybrid model captures the transition between SSA and SIA in a less computationally intensive way than full-Stokes simulations, but remains a predominantly numerical technique. Here we mathematically analyse the 'L1L2' method to derive simple, yet more accurate expressions for the ice velocity and flux in this transitional regime.

In this paper, we look at the flow of shear-thinning ice over a bed of uniform shear strength, through a wide, shallow rectangular stream. We use asymptotic analysis to derive closed-form expressions for the velocity field and flux through the stream, both when basal resistance is small and as it increases towards the driving stress. We show that these expressions recover both the SSA and SIA limits as expected, but we also obtain a new, intermediate regime in which basal shear-softening is significant. We further solve for the flow-field numerically, confirming the existence of this regime, and show that our new expression significantly reduces the error in predicted velocities.

2. Governing equations and approach

We consider the steady flow of shear-thinning ice in a shallow, rectangular channel of depth H and half-width W which is uniform in the along-flow direction, with equal bed and surface slopes (Fig. 1). This means the pressure is hydrostatic, and the velocity field is only in the along-stream direction, $\mathbf{u} = (u(y, z), 0, 0)$. As the flow is uniform in this direction, we have no extensional strains in this geometry, a simplification that allows us to retain and evaluate the impact of vertical strain instead. While longitudinal and vertical strains can become comparable if basal resistance is very low and the along-stream variation is large, along-stream changes in velocity often occur over length scales much greater than the width or depth of ice streams, with extensional stresses effectively acting to smooth variations in driving stress (Kamb and Echelmeyer, 1986).

Given these assumptions, the stress field $\boldsymbol{\tau}$ within the ice satisfies

$$\frac{\partial \tau_{xy}}{\partial y} + \frac{\partial \tau_{xz}}{\partial z} = -\frac{\tau_d}{H}, \tag{1}$$

where the driving stress,

$$\tau_d = \rho_i g H \frac{\partial S}{\partial x}, \tag{2}$$

is due to gradients in surface height S, density of ice ρ_i and gravitational acceleration g. We take a power-law shear-thinning

rheology for the ice

$$e_{ij} = A\tau^{n-1}\tau_{ij}, \quad e_{ij} = \frac{1}{2}\left(\nabla \mathbf{u} + \nabla \mathbf{u}^T\right), \quad \tau = \sqrt{\frac{1}{2}\tau_{ij}\tau_{ij}}, \tag{3}$$

where A is the viscosity prefactor, which in general may be a function of temperature and grain size, but here we take as constant. The shear-thinning exponent n is usually taken to be 3 for ice (Glen, 1955), although using values from 1.8 to 4 represents the different modes of deformation that make up ice flow (Goldsby and Kohlstedt, 2001; Millstein and others, 2022). Even higher effective shear exponents could represent the effect of damage or shear heating in the margins of the ice stream, where high shear rates warm and soften the ice further (Minchew and others, 2017). We will show numerical results for $n = 3$, but give expressions for general n as far as practical.

2.1. Boundary conditions

On the two sidewalls at $y = \pm W$ we apply a no-slip boundary condition, motivated by the fact that ice streams and glaciers are usually either topographically constrained between high bedrock or surrounded by nearly stagnant ice. At the upper surface of the ice, $z = H$, we impose a no-stress condition as the ice is in contact with the atmosphere. At the base of the stream $z = 0$, we link the basal shear stress, $\tau = \tau_b$, to the basal sliding speed, $u = u_b$, through a sliding law representing the rheology and/or geometry of the bed in contact with the base of the ice stream.

Over beds of deformable sediment, an appropriate basal boundary condition is a plastic traction law,

$$\begin{aligned} \tau_b &= \mu N, \quad u_b > 0, \\ \tau_b &< \mu N, \quad u_b = 0, \end{aligned} \tag{4}$$

where μ is a friction coefficient and $N = p_i - p_w$ is the effective pressure, which is the difference between the pressure exerted by the weight of the ice p_i and the water pressure at the sliding surface p_w. This will form the basis for our analysis here, since deformable sediments are found below many fast-flowing streams (Kamb, 2001; Iverson, 2010).

In large-scale models, the basal shear stress and sliding speed are often related via a power-law,

$$\tau_b = C u_b^{1/m}, \tag{5}$$

originally derived from ice sliding over a hard bed with small-scale topography (Weertman, 1957) but presently extended to other scenarios by modifying the value of the exponent m. Large values of $m \geq 8$ have been used to approximate plastic deformation (Rosier and others, 2015; Minchew and others, 2016; Joughin and others, 2019). A numerical study of the impact of this power-law sliding in a similar channel geometry is given in Adhikari and Marshall (2012), and we will discuss the value of our plastic bed calculations for reproducing these results.

If the basal shear strength is large compared to the driving stress τ_d, (4) reduces to a bed that is unyielded everywhere, and we obtain a no-slip boundary condition, $u_b = 0$, as would be the case in the SIA. When $\tau_b \to 0$, we recover a no-stress basal boundary condition, where the SSA is strictly valid. In this paper, we recover both of these well-known limits but focus on the intermediate regime where both u_b/u_s (u_s the surface speed) and τ_b/τ_d are large. We seek to find closed-form approximations for the ice velocity field, in particular the surface speed u_s (which is most readily observable), basal sliding u_b and total ice flux Q, as a function of the width W and height H of the stream, the
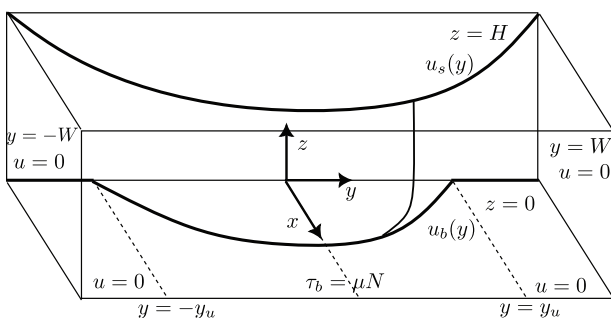

Figure 1. Diagram of the ice stream geometry, showing the $u = 0$ boundary condition on the sidewalls $y = \pm W$, the surface velocity profile $u_s(y)$ at $z = H$, the profile of sliding speed $u_b(y)$ at $z = 0$, and the point at $y = y_u$ marking the changeover in basal boundary condition from $\tau_b = \mu N$ in the central region to $u_b = 0$ close to the sidewalls. An example vertical velocity profile is drawn to show the concentration of vertical shear close to the bed.

shear thinning exponent n and the ratio of basal shear stress to driving stress τ_b/τ_d.

Our reference point will be the expressions for centreline surface velocity u_{mid} and flux Q obtained by simply summing the SIA and SSA results for flow through a uniform ice stream (Raymond, 1996; Cuffey and Paterson, 2010),

$$u_{mid}^0 = \frac{2AH}{n+1}\left[(\tau_d - \mu N)^n \frac{W^{n+1}}{H} + \mu N^n\right], \qquad (6)$$

$$Q^0 = \frac{4AH^2}{n+2}\left[(\tau_d - \mu N)^n \frac{W^{n+2}}{H} + \mu N^n \frac{W}{H}\right], \qquad (7)$$

which neglect the effect of basal shear softening. Our goal is to improve on the accuracy of these results while still retaining a readily useable closed-form expression.

3. Numerical method

We numerically solve for the flow of ice in a rectangular channel with variable basal traction to assess the accuracy of our asymptotic expressions. We use COMSOL to solve (1) in the half-channel $0 < y < W$, $0 < z < H$, invoking the symmetry of the flow, as a generalised Poisson equation for u. The effective viscosity is regularised by the addition of a small constant $\epsilon_1 = 10^{-9}$ to prevent divergence at $z = H$, $y = 0$,

$$\nabla \cdot \left[\frac{1}{2A}(\tau_{xz}^2 + \tau_{xy}^2 + \epsilon_1)^{(1-n)/2}\nabla u\right] = -\frac{\tau_d}{H}. \qquad (8)$$

The boundary conditions are no-stress on $y = 0$ and $z = H$, no-slip on $y = W$ and a traction law on $z = 0$ that represents a regularised form of (4),

$$\tau_{xz} = \mu N \tanh\left(\frac{u}{\epsilon_2}\right). \qquad (9)$$

We used an automatically generated triangular mesh on COMSOL's extra-fine setting (5 grid points across the depth of the stream), and with relative error for convergence of 10^{-5}. The regularisation parameters $\epsilon_1 = 10^{-9}$ and $\epsilon_2 = 10^{-4}$ were

also chosen such that decreasing their value by an order of magnitude did not affect the calculated velocities by more than a factor of 10^{-5}. Using the finest available mesh setting also did not affect calculated velocities by more than a factor of 2×10^{-4} as compared to the extra-fine setting.

The numerical results are not the focus of this work but serve as a benchmark for our derived expressions for velocity and flux, as described in the following sections.

4. Mathematical method

To begin our mathematical analysis, we start by depth-integrating (1) to get

$$\frac{\partial}{\partial y}\int_0^z \tau_{xy}\,dz + \tau_{xz} - \tau_b = -\tau_d\frac{z}{H}, \qquad (10)$$

where τ_b appears as the integration constant found by evaluating this expression at $z = 0$. Evaluating (10) at $z = H$, where $\tau_{xz} = 0$, we find that

$$\frac{\partial}{\partial y}\int_0^H \tau_{xy}\,dz - \tau_b = -\tau_d. \qquad (11)$$

Where the bed is yielded, so that $\tau_b = \mu N$ uniformly, we can integrate across the stream to arrive at

$$-(\tau_d - \mu N)y = \int_0^H \tau_{xy}\,dz, \qquad (12)$$

and so the problem reduces to evaluating the depth-integrated lateral shear stress, and in particular evaluating the relative effects of vertical and lateral shear on the viscosity.

4.1. Approximation of vertical shear stress and viscosity

If basal sliding is significant across the width of the channel, we assume that gradients in the surface velocity profile $u_s(y)$ provide an accurate reflection of the lateral shear rate throughout the full depth of the ice.

Motivated by numerically calculated stress fields (Fig. 2), the much larger horizontal than vertical lengthscales, and the
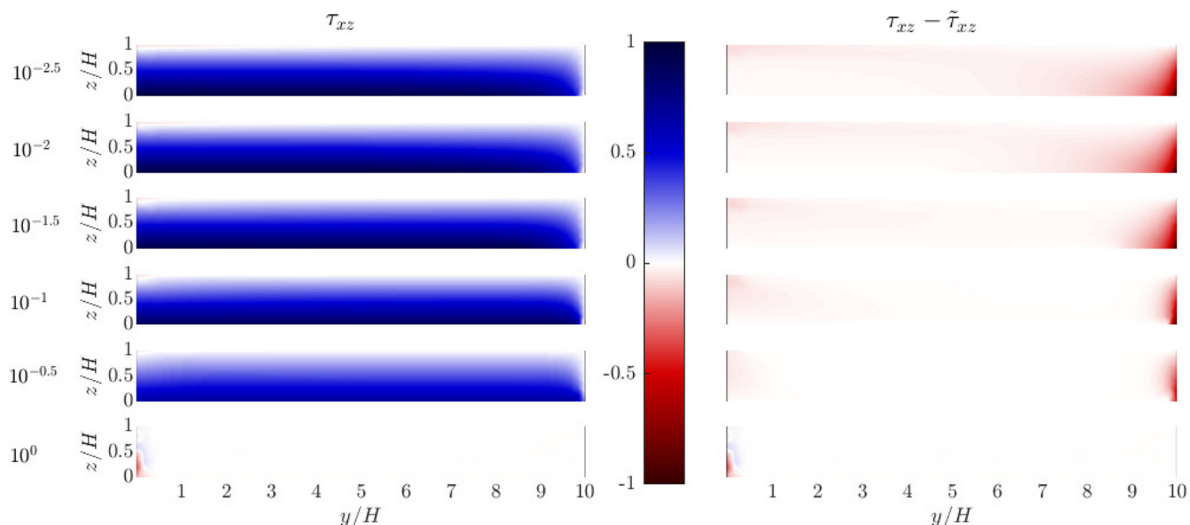

Figure 2. Left, numerically calculated τ_{xz}, and right, difference between τ_{xz} and the approximation $\tilde{\tau}_{xz}$ (13), for increasing values of $1 - \mu N/\tau_d = 10^{-2.5}$, 10^{-2}, $10^{-1.5}$, 10^{-1}, $10^{-0.5}$, 1. All values are scaled so that $\tau_d = 1$. The agreement is generally excellent, but τ_{xz} is noticeably less than $\tilde{\tau}_{xz}$ in a region $O(H)$ near the sidewall, and over unyielded regions of the bed where $\tau_b < \mu N$. Near the centre of the stream the divergence of viscosity leads to error in the numerically calculated field (particularly visible when $\mu N = 0$ and the exact solution is $\tau_{xz} = 0$ everywhere). All for $W/H = 10$ and $n = 3$.

approach of Hindmarsh ([2004]), we further assume that the vertical shear stress that feeds into the rheology is approximately linear with depth. Hence we may approximate the lateral and vertical shear stresses, and hence the ice rheology, as

$$\tau_{xy} = \tilde{\eta}\frac{\partial u_s}{\partial y}, \quad \tilde{\tau}_{xz} = \tilde{\eta}\frac{\partial u}{\partial z} = \mu N \frac{H-z}{H}, \quad (13)$$

$$\tilde{\eta} = \frac{1}{2A}\left(\tilde{\tau}_{xz}^2 + \tau_{xy}^2\right)^{(1-n)/2}, \quad (14)$$

where the tilde denotes that this is now based on the approximate vertical shear stress, so e.g. $\tilde{\eta}$ is the approximate ice viscosity. This is similar to the L1L2 model of Hindmarsh ([2004]) but here vertical shear stresses are scaled with μN rather than τ_d.

4.2. Horizontal shear rate

Writing $\tilde{\eta} = \tau_{xy}/\frac{\partial u_s}{\partial y}$, we can approximate Eqns. (13)–(14) in two limits depending on the relative sizes of τ_{xy} and $\tilde{\tau}_{xz}$. If vertical shear stresses are much greater than horizontal, $\tilde{\tau}_{xz} \gg \tau_{xy}$,

$$\tau_{xy} \approx \left(\mu N \frac{H-z}{H}\right)^{1-n}\frac{1}{2A}\frac{\partial u_s}{\partial y}, \quad (15)$$

which exhibits strong depth-dependence. In contrast, if lateral shear stresses are much greater than vertical, $\tau_{xy} \gg \tilde{\tau}_{xz}$,

$$\tau_{xy} \approx \left(\frac{1}{2A}\frac{\partial u_s}{\partial y}\right)^{1/n}, \quad (16)$$

which is uniform in depth.

We define a transition depth z_t at which a transition in the dominant stress occurs, and below which basal shear dominates, given by

$$\left(\mu N \frac{H-z_t}{H}\right) \sim \left(\frac{1}{2A}\frac{\partial u_s}{\partial y}\right)^{1/n}. \quad (17)$$

Note that in regions where the lateral stress is large, basal shear never dominates and z_t would be negative. Thus, we have two regimes depending on the sign of z_t. Where lateral stresses are smaller than μN, the leading order expression for the depth-integrated stress is given by integrating the dominant term on either side of z_t, so starting from (12) we have

$$-(\tau_d - \mu N)y = \int_0^H \tau_{xy}\,\mathrm{d}z \quad (18)$$

$$= \int_{z_t}^H \left(\frac{1}{2A}\frac{\partial u_s}{\partial y}\right)^{1/n}\mathrm{d}z + \int_0^{z_t}\left(\mu N \frac{H-z}{H}\right)^{1-n}\frac{1}{2A}\frac{\partial u_s}{\partial y}\,\mathrm{d}z \quad (19)$$

$$= (H-z_t)\left(\frac{1}{2A}\frac{\partial u_s}{\partial y}\right)^{1/n} + \frac{H}{(n-2)\mu N}\left(\mu N \frac{H-z_t}{H}\right)^{2-n}\frac{1}{2A}\frac{\partial u_s}{\partial y}$$
$$- \frac{H(\mu N)^{1-n}}{n-2}\frac{1}{2A}\frac{\partial u_s}{\partial y} \quad (20)$$

$$\sim \frac{n-1}{n-2}\frac{H}{\mu N}\left(\frac{1}{2A}\frac{\partial u_s}{\partial y}\right)^{2/n} \quad \text{if} \quad \frac{\partial u_s}{\partial y} \ll 2A(\mu N)^n, \quad (21)$$

while if $z_t \leq 0$ then lateral shear dominates the viscosity everywhere, so

$$-(\tau_d - \mu N)y = \int_0^H \tau_{xy}\,\mathrm{d}z = \int_0^H\left(\frac{1}{2A}\frac{\partial u_s}{\partial y}\right)^{1/n}\mathrm{d}z \quad (22)$$

$$= H\left(\frac{1}{2A}\frac{\partial u_s}{\partial y}\right)^{1/n} \quad \text{if} \quad \frac{\partial u_s}{\partial y} > 2A(\mu N)^n. \quad (23)$$

If $\mu N \ll \tau_d$, then (23) applies almost everywhere and the leading order expression for the surface velocity profile is given by

$$u_s \approx \frac{2A}{(n+1)}\frac{(\tau_d - \mu N)^n}{H^n}\left[W^{n+1} - y^{n+1}\right], \quad (24)$$

which is the SSA approximation for an ice stream with constant basal traction μN (Raymond, [1996]). While the modification to τ_d is negligible in the limit for which (24) is asymptotically valid, this expression is used even when $\mu N \sim \tau_d$ (e.g. Minchew and others, [2018]).

However, as basal drag increases, the vertical shear stress starts to dominate in the central region of the stream where lateral stresses are lowest. This shear-softening decreases the depth-integrated viscosity, and leads to a significant increase in velocity compared to the prediction of the SSA approach when $(\tau_d - \mu N)W \sim \tau_d H$ ([Fig. 3]).

The SSA result becomes an even poorer approximation as basal drag increases further, and the bed becomes unyielded over a significant portion of the stream. Using (12), which assumes that $\tau_b = \mu N$ everywhere, overestimates the resistance to flow and thus additionally underestimates the ice velocity; to correct this we must look further at the vertical structure of the flow.

4.3. Vertical shear rate and basal boundary condition

Now that we have a measure of both τ_{xy} and τ_{xz}, we can calculate the effective viscosity and thus evaluate the vertical deformation of the ice by finding $\partial u/\partial z$. This allows us to estimate the basal velocity u_b and to better characterise whether the bed should be yielded ($\tau_b = \mu N$) or unyielded ($u_b = 0$).

At the sides of the stream, where lateral shear dominates the viscosity, and still approximating the vertical shear stress as linear in depth, we can use (13) solve for the approximate vertical shear,

$$\frac{\partial u}{\partial z} \approx \frac{\tilde{\tau}_{xz}}{\tilde{\eta}} = \mu N \frac{H-z}{H}\left(\frac{1}{2A}\left[(\tau_d - \mu N)\frac{y}{H}\right]^{1-n}\right)^{-1}, \quad (25)$$

and then integrating this vertical shear rate down from the surface we obtain a velocity field

$$u = u_s(y) - \frac{2A}{2}\mu N \frac{(H-z)^2}{H}\left[(\tau_d - \mu N)\frac{y}{H}\right]^{n-1}, \quad (26)$$

resulting in a basal sliding speed

$$u_b(y) = \frac{2AH(\tau_d - \mu N)^n}{(n+1)}\left[\left(\frac{W}{H}\right)^{n+1} - \left(\frac{y}{H}\right)^{n+1} - \frac{(n+1)\mu N}{2(\tau_d - \mu N)}\left(\frac{y}{H}\right)^{n-1}\right]. \quad (27)$$
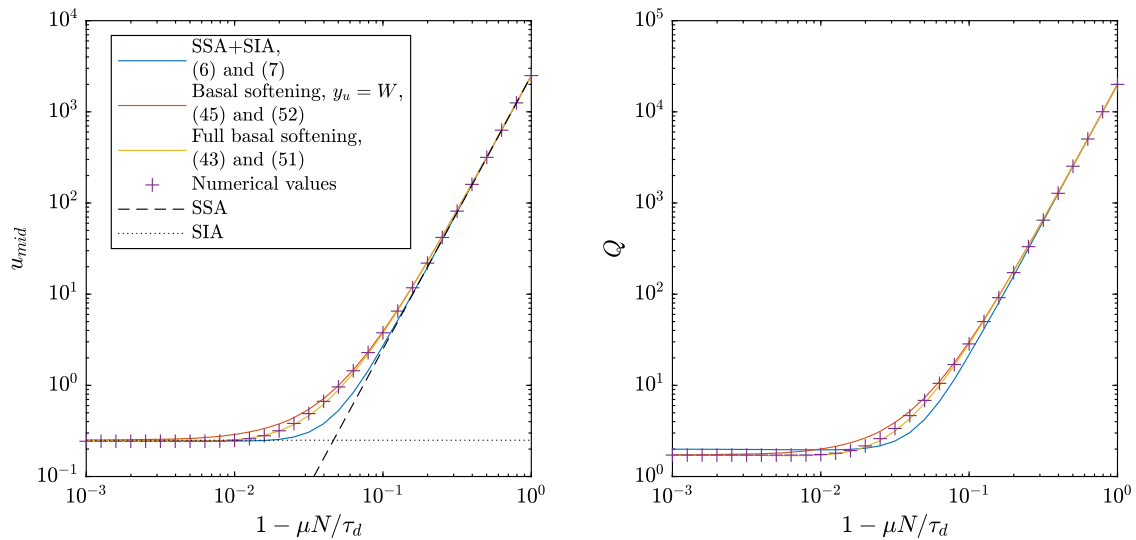
Figure 3. Including shear softening improves the match to numerically calculated values of (a) the centreline surface velocity $u_s(0)$ and (b) the total flux Q, particularly when $\tau_d - \mu N \sim 0.1\tau_d$. Here $W = 10H$ and $n = 3$. SSA and SIA limits of the surface velocity are shown as dashed and dotted lines.

Note that this becomes negative very close to $y = W$; in effect this determines the point beyond which the bed is unyielded and $u_b = 0$ should apply instead of $\tau_b = \mu N$. We can find the approximate edge of the unyielded region $y = y_u$ by solving $u_b(y_u) = 0$, so that

$$W^{n+1} = y_u^{n+1} + \frac{(n+1)\mu N H^2}{2(\tau_d - \mu N)} y_u^{n-1}. \qquad (28)$$

To leading order in $W - y_u$ we can solve for y_u approximately and get

$$y_u = W - \frac{\mu N H^2}{2(\tau_d - \mu N)W}, \qquad (29)$$

which, for its simplicity, we will take through the rest of the paper in all calculations and plots using y_u. Figure 4 shows that (29) accurately captures the behaviour as $y_u \to W$, as well as agreeing that $y_u \to 0$ as $\mu N \to \tau_d$, but determining the exact boundary of the yielded bed is a free boundary problem (Schoof, 2006) and in general can only be solved for numerically, and hence expressions left in terms of y_u could be improved with higher-order calculations of this yield boundary's location.

To find the internal deformation in the centre of the stream, where basal shear begins to affect the ice viscosity, there are
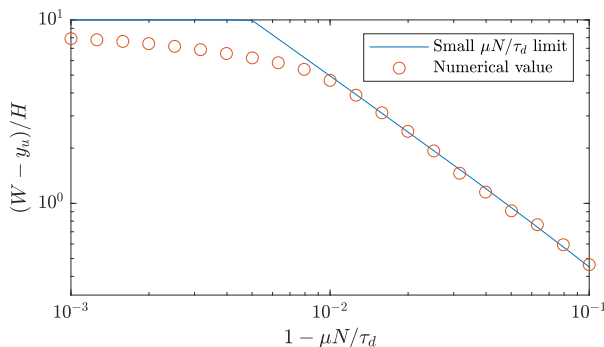

Figure 4. Match between the approximate expression for y_u (29), and the numerically calculated edge of the yielded bed, for $W = 10H$, $n = 3$. The disagreement at larger μN is expected since when y_u moves away from the sidewalls the approximations that lead to (28) no longer hold, but (29) does capture that $y_u \to 0$ there, in agreement with numerical results.

two regimes to consider: below z_t the basal shear dominates, while close to the surface the lateral shear sets the viscosity. Considering only these dominant contributions to the viscosity, we can obtain the leading order approximation to $\partial u/\partial z$ above z_t by

$$\frac{\partial u}{\partial z} \approx \frac{\tilde{\tau}_{xz}}{\tilde{\eta}}$$

$$= \mu N \frac{H - z}{H} \left(\frac{1}{2A} \left[\frac{n-2}{n-1} \mu N(\tau_d - \mu N) \frac{y}{H} \right]^{1-n/2} \right)^{-1}, \qquad (30)$$

where $z > z_t$,

so that the velocity field, found by integrating down from the surface profile, is given by

$$u = u_s(y) - \frac{2A}{2} \mu N \frac{(H-z)^2}{H} \left[\frac{n-2}{n-1} \mu N(\tau_d - \mu N) \frac{y}{H} \right]^{(n-1)/2}, \qquad (31)$$

in particular at $z = z_t$ where

$$u(z_t) = u_s(y) - \frac{2A}{2} \frac{H}{\mu N} \left[\frac{n-2}{n-1} \mu N(\tau_d - \mu N) \frac{y}{H} \right]^{(n+1)/2}. \qquad (32)$$

To continue down below z_t, where the leading order form of the viscosity is dominated by basal drag, we similarly calculate the vertical shear as

$$\frac{\partial u}{\partial z} \approx \frac{\tilde{\tau}_{xz}}{\tilde{\eta}} = \tilde{\tau}_{xz} \left(\frac{1}{2A} \tilde{\tau}_{xz}^{1-n} \right)^{-1} = 2A \left(\mu N \frac{H-z}{H} \right)^n, \qquad (33)$$

where $z < z_t$,

then integrate down from $z = z_t$ to find

$$u = u(z_t) - \frac{2A}{n+1} \mu N^n H \left[\left(\frac{H-z}{H} \right)^{n+1} - \left(\frac{n-2}{n-1} \frac{\tau_d - \mu N}{\mu N} \frac{y}{H} \right)^{(n+1)/2} \right]. \qquad (34)$$

Thus, the basal velocity is

$$u_b = u_s(y) - \frac{2A}{n+1} H \mu N^n \left[1 + \frac{n-1}{2} \left(\frac{n-2}{n-1} \frac{\tau_d - \mu N}{\mu N} \frac{y}{H} \right)^{(n+1)/2} \right].$$

(35)

Note that the deformation velocity, $u_d = u_s - u_b$ is

$$u_d = \frac{2A}{n+1} H \mu N^n \left[1 + \frac{n-1}{2} \left(\frac{n-2}{n-1} \frac{\tau_d - \mu N}{\mu N} \frac{y}{H} \right)^{(n+1)/2} \right]. \quad (36)$$

The prefactor is the SIA surface speed, and the second term inside the brackets is much less than 1 until the very edges of this central, basal drag dominated region. Similarly the deformation flux q_d, the integral of $u(z) - u_b$ through the depth of the stream, is dominated by the SIA term so

$$q_d \approx \frac{2A}{n+2} H^2 \mu N^n. \quad (37)$$

5. Results

5.1. Surface velocity and sliding speed

Surface velocity is the primary observation available to constrain ice dynamics and basal processes, while sliding speed is a key determinant of the total flux through the ice stream. We now combine our expressions for stress and velocity to obtain the surface velocity at the centreline of the ice stream. We have calculated the horizontal shear rate over the yielded regions where $\tau_b = \mu N$, the extent y_u of the unyielded region of the bed, and the vertical shear at the edge of this region, where both $u_b = 0$ and $\tau_b = \mu N$. Thus, we integrate up from the bed at y_u to find $u_s(y_u)$, then integrate inwards to find the surface velocity profile over the yielding region, giving

$$u_{mid} = \int_0^H \frac{\partial u}{\partial z} \bigg|_{y=y_u} dz + \int_0^{y_u} \frac{\partial u_s}{\partial y} dy. \quad (38)$$

There are two regimes to consider depending on the dominant contribution to the depth-integrated viscosity at y_u. When the basal drag is small, (23) dominates and we have a small modification to the SSA solution,

$$u_s \approx 2AH \frac{(\tau_d - \mu N)^n}{n+1} \left[\left(\frac{y_u}{H} \right)^{n+1} - \left(\frac{y}{H} \right)^{n+1} + \frac{\mu N}{2(\tau_d - \mu N)} \left(\frac{y_u}{H} \right)^{n-1} \right],$$

(39)

Since y_u is very close to W, and $\tau_d - \mu N \gg \mu N$, the deformation velocity is small compared to the horizontal shear and so that the leading order expression for the centreline velocity is exactly the SSA result of

$$u_{mid} \approx 2AH \frac{(\tau_d - \mu N)^n}{n+1} \left(\frac{W}{H} \right)^{n+1}, \quad (40)$$

and this is also the leading order term in u_b.

When the basal drag is large, (21) dominates the horizontal shear, and so

$$u_b \approx \frac{4AH}{n+2} \left(\frac{n-2}{n-1} \mu N(\tau_d - \mu N) \right)^{n/2} \left[\left(\frac{y_u}{H} \right)^{(n+2)/2} - \left(\frac{y}{H} \right)^{(n+2)/2} \right]$$

(41)

and thus

$$u_{mid} \approx 2AH \left[\frac{2}{n+2} \left(\frac{n-2}{n-1} \mu N(\tau_d - \mu N) \right)^{n/2} \left(\frac{y_u}{H} \right)^{(n+2)/2} + \frac{\mu N^n}{n+1} \right].$$

(42)

Using the expression for y_u from (29), we find that (42) provides a good match to the numerical results when $\tau_d - \mu N \ll \tau_d$ (Fig. 5).

We suggest that an appropriate expression for the centreline velocity that transitions smoothly between the two regimes can be found by adding together (40) and (42), giving

$$u_{mid} \approx 2AH \left[\frac{(\tau_d - \mu N)^n}{n+1} \left(\frac{W}{H} \right)^{n+1} \right.$$
$$\left. + \frac{2}{n+2} \left(\frac{n-2}{n-1} \mu N(\tau_d - \mu N) \right)^{n/2} \left(\frac{y_u}{H} \right)^{(n+2)/2} + \frac{\mu N^n}{n+1} \right].$$

(43)

We see that the first term, which dominates when $\mu N \ll \tau_d$, is the SSA expression, while the final term, which remains when $\tau_d = \mu N$, is the SIA expression. In effect, we have introduced a new term to represent the intermediate regime, in which basal drag is significant enough to affect the viscosity, while basal sliding remains high enough to affect the surface velocity. Using (29) as the approximation for y_u, this becomes a closed-form expression for the surface velocity as a function of basal strength which could be readily used as a lumped description of ice stream dynamics in a model of wider climate processes. The corresponding expression for the sliding speed at the centre of the stream is found by subtracting off the deformation velocity,

$$u_b(0) \approx 2AH \left[\frac{(\tau_d - \mu N)^n}{n+1} \left(\frac{W}{H} \right)^{n+1} \right.$$
$$\left. + \frac{2}{n+2} \left(\frac{n-2}{n-1} \mu N(\tau_d - \mu N) \right)^{n/2} \left(\frac{y_u}{H} \right)^{(n+2)/2} \right].$$

(44)

We also consider a further simplification to (43) by approximating y_u as W,

$$u_{mid}^+ = 2AH \left[\frac{(\tau_d - \mu N)^n}{n+1} \left(\frac{W}{H} \right)^{n+1} \right.$$
$$\left. + \frac{2}{n+2} \left(\frac{n-2}{n-1} \mu N(\tau_d - \mu N) \right)^{n/2} \left(\frac{W}{H} \right)^{(n+2)/2} + \frac{\mu N^n}{n+1} \right],$$

(45)

This will systematically overestimate the surface velocity, but in wide channels, this can still provide an improved match to the numerical results compared to neglecting the basal shear-thinning entirely (Fig. 5).

Figure 5 shows the difference between the numerically calculated values of u_{mid} and the three approximations: SIA plus SSA, (45) and (43). SIA plus SSA significantly underestimates the centreline velocity for wide streams with intermediate sliding rates – clearly showing that SSA is valid when $\mu N/\tau_d \ll 1$, while SIA is valid when $\mu N/\tau_d \gg H/W$, missing the intermediate regime if $W \gg H$, where the errors can be upwards of 40%. As expected, (45) is an overestimate but increasingly close to the numerical results as W/H increases. (43) provides the closest match to the numerical results, remaining within 10% of the calculated values and only significantly deviating where $W/H < 5$ and the shallow approximations break down.
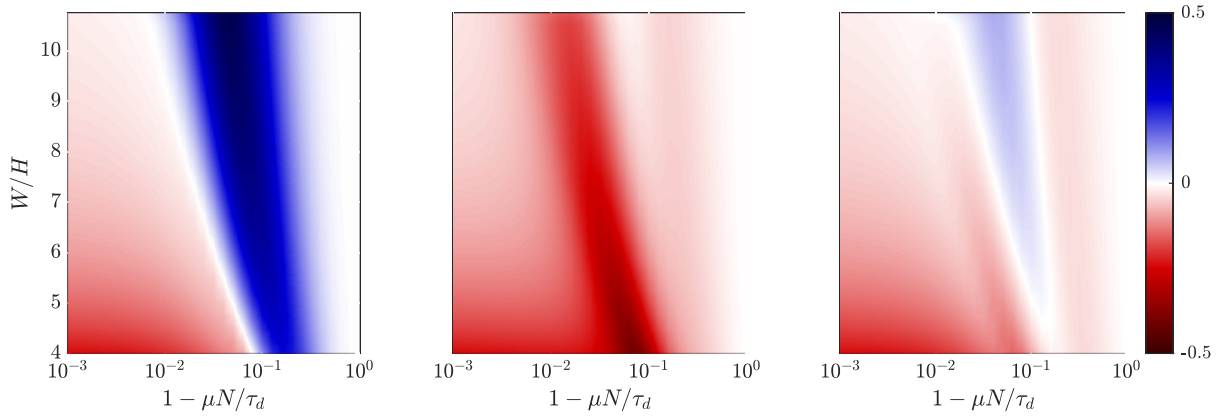
Figure 5. Fractional error in expressions for u_{mid} as compared to the numerically calculated values (1 – expression/numerical value, so overestimates are negative errors), for a range of aspect ratios and basal strengths, with $n = 3$. (a) Sum of SIA and SSA, Eqn. (6), (b) including basal shear softening, but with y_u set to W (45), and (c) the full expression (43) using (29) for y_u. Both (b) and (c) represent improvements over (a), with (c) the closest match to the numerical results. When the aspect ratio is not large, all the approximations start to break down. The maximum error in (b) is −0.40 at $W/H = 4$ but reduces to −0.17 at $W/H = 11$. The error in (c) ranges from −0.24 to 0.085 but remains within ±0.1 for $W/H > 5.75$.

5.2. Total flux

While surface velocity is most easily measurable, the evolution of ice stream thickness depends on the total flux through the stream. We now calculate the ice flux through the stream, again considering the two regimes depending on the size of μN compared to τ_d.

When μN is small, vertical deformation is negligible, and so the total flux Q is found by integrating $u_s H$ across the width of the stream, with u_s given by (39). Thus, we recover the SSA result,

$$Q = 4AH^2 \int_0^W \frac{(\tau_d - \mu N)^n}{n+1} \left[\left(\frac{W}{H} \right)^{n+1} - \left(\frac{y}{H} \right)^{n+1} \right] \mathrm{d}y$$

$$= 4AH^3 \frac{(\tau_d - \mu N)^n}{n+2} \left(\frac{W}{H} \right)^{n+2}. \tag{46}$$

However, if the bed is strong, we divide the flux between the region over the yielded bed, and the region over the unyielded margins. Over the central, yielded region, we have contributions to the flux from both the basal sliding (41), and the internal deformation (37), such that

$$Q_{inner} = 4AH^2 \int_0^{y_u} \frac{\mu N^n}{n+2} + \frac{2}{n+2} \left(\frac{n-1}{n-2} \mu N(\tau_d - \mu N) \right)^{n/2}$$

$$\times \left[\left(\frac{y_u}{H} \right)^{(n+2)/2} - \left(\frac{y}{H} \right)^{(n+2)/2} \right] \mathrm{d}y$$

$$= 4AH^3 \left[\frac{\mu N^n}{n+2} \frac{y_u}{H} + \frac{2}{n+4} \left(\frac{n-1}{n-2} \mu N(\tau_d - \mu N) \right)^{n/2} \right.$$

$$\left. \times \left(\frac{y_u}{H} \right)^{n+4/2} \right]. \tag{47}$$

In the margins, we have $u_b = 0$ and large vertical shear stress. While lateral shear will start to dominate in a region of order H close to the sidewalls, until then the SIA holds and the velocity is approximately y-independent, with

$$u = \frac{2AH\tau_b^n}{n+1} \left(\frac{z}{H} \right)^{n+1}. \tag{48}$$

Thus, the flux in this outer region is approximately given by

$$Q_{outer} = \frac{4AH^2 \tau_b^n}{n+2} (W - \alpha H - y_u), \tag{49}$$

where the $-\alpha H$ represents the reduced flux due to matching onto the no-slip sidewalls. On dimensional grounds, we anticipate that the sidewall correction should tend to a constant multiple of H as W increases. Numerically, it appears that $\alpha \approx 1.4$ (Fig. 6). While in the asymptotic limit of $W \gg H$, this correction is negligible, for moderately wide channels the inclusion of this term provides a simple increase in the accuracy of our expression (Fig. 7). Further analytic progress in this regime is beyond the scope of this paper, and further numerical calculations of the non-sliding regime (taking instead a shape factor-based approach to the effect of the sidewalls) are found in Nye (1965). For wide channels, this is a small correction, and we are primarily interested in the more rapidly sliding regime.

The total flux through the ice stream in the high basal drag regime therefore is approximately given by

$$Q = 4AH^3 \left[\frac{\mu N^n}{n+2} \frac{W - \alpha H}{H} \right.$$

$$\left. + \frac{2}{n+4} \left(\frac{n-1}{n-2} \mu N(\tau_d - \mu N) \right)^{n/2} \left(\frac{y_u}{H} \right)^{n+4/2} \right]. \tag{50}$$

Again we suggest that summing the fluxes derived from each limit gives a single expression that transitions accurately between regimes, so

$$Q = 4AH^3 \left[\frac{\mu N^n}{n+2} \frac{W - \alpha H}{H} + \frac{2}{n+4} \left(\frac{n-1}{n-2} \mu N(\tau_d - \mu N) \right)^{n/2} \right.$$

$$\left. \times \left(\frac{y_u}{H} \right)^{n+4/2} + \frac{(\tau_d - \mu N)^n}{n+2} \left(\frac{W}{H} \right)^{n+2} \right]. \tag{51}$$

As shown in Figure 7, this expression is within 10% of the numerically calculated results, far better than just summing the SSA and SIA values.
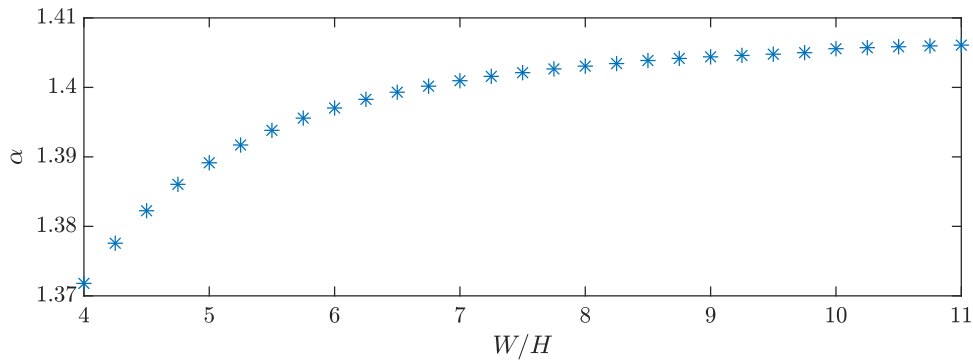
Figure 6. With a no-slip base, the effect of the sidewalls on the flux as summarised by the value of α in Eqn. (49) tends towards a constant value as W/H increases.
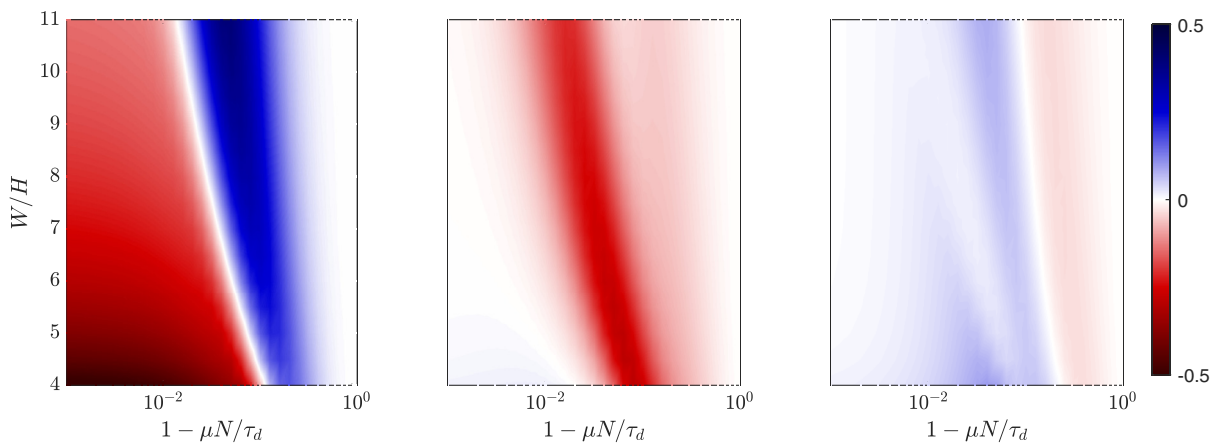

Figure 7. Fractional error in expressions for Q as compared to the numerically calculated values, for a range of aspect ratios and basal strengths, with $n = 3$. (a) Sum of SIA and SSA, Eqn. (7) – note this does not include the sidewall modification to the SIA flux, (b) including basal shear softening, but with y_u set to W (52), and (c) the full expression (51) using (29) for y_u. Both (b) and (c) represent improvements over (a), with (c) the closest match to the numerical results. To guide the eye, the fractional error in (b) ranges from -0.29 (at the smallest values of W/H) to 0.017 and in (c) from -0.036 to 0.098.

As before, a simpler version using $y_u \approx W$ is given by

$$Q_+ = 4AH^3 \left[\frac{\mu N^n}{n+2} \frac{W - \alpha H}{H} + \frac{2}{n+4} \left(\frac{n-1}{n-2} \mu N(\tau_d - \mu N) \right)^{n/2} \right.$$

$$\left. \times \left(\frac{W}{H} \right)^{n+4/2} + \frac{(\tau_d - \mu N)^n}{n+2} \left(\frac{W}{H} \right)^{n+2} \right],$$

(52)

and can also provide a good approximation to the numerical results, particularly for wide streams (Fig. 7b). However, it is always an overestimate. By contrast, neglecting basal shear-thinning by setting $y_u = 0$ and simply summing the SSA and SIA expressions is an underestimate that captures the intermediate regime increasingly poorly for wider streams (Fig. 7a).

5.3. Cross-stream surface velocity profiles

The surface velocity profile reveals more information about the bed and ice rheology than the centre-line speed alone. In our numerical results, we see appreciable changes in surface velocity profile as the bed strength increases (Fig. 8), with the width of the central region of quasi-uniform velocity first narrowing in the intermediate regime and then increasing to almost the full width of the stream in the SIA limit.

As previously noted, a calculation of the velocity field close to the sidewalls, over the unyielded sections of the bed, is beyond the scope of our present analysis (see also the discussion section). Thus, to

explain the full surface velocity profiles including the shear margins, we rely on the numerically calculated profiles for the $u_b = 0$ limit.

Initially, as the basal drag increases, basal shear-softening reduces the effective viscosity in the centre of the stream, leading to larger shear rates there, and more rounded velocity profiles $(u_{mid} - u_s \sim y^{(n+2)/2})$ compared to the freely sliding case $(u_{mid} - u_s \sim y^{n+1})$. As bed strength increases further, the unyielded regions of the bed encroach towards the centre of the stream. The shear margins are concentrated over the non-sliding regions (c.f. Truffer and others, 2001), and numerically we see that the shape of these margins closely resembles surface velocity profile for a completely static bed. We therefore suggest that an approximate expression for the surface velocity profile over the entire stream can be found, similarly to the method by which the centre-line velocity was found in (43), by summing the SSA solution, the numerically calculated profile for non-sliding bed, and a term representing effect of basal shear softening where $y < y_u$ (using (29) for y_u),

$$u_s(y) \approx u_s(y, u_b = 0) + 2AH \frac{(\tau_d - \mu N)^n}{n+1} \left[\left(\frac{W}{H} \right)^{n+1} - \left(\frac{y}{H} \right)^{n+1} \right]$$

$$+ \frac{4AH}{n+2} \left(\frac{n-2}{n-1} \mu N(\tau_d - \mu N) \right)^{n/2}$$

$$\times \max \left[\left(\frac{y_u}{H} \right)^{(n+2)/2} - \left(\frac{y}{H} \right)^{(n+2)/2}, 0 \right].$$
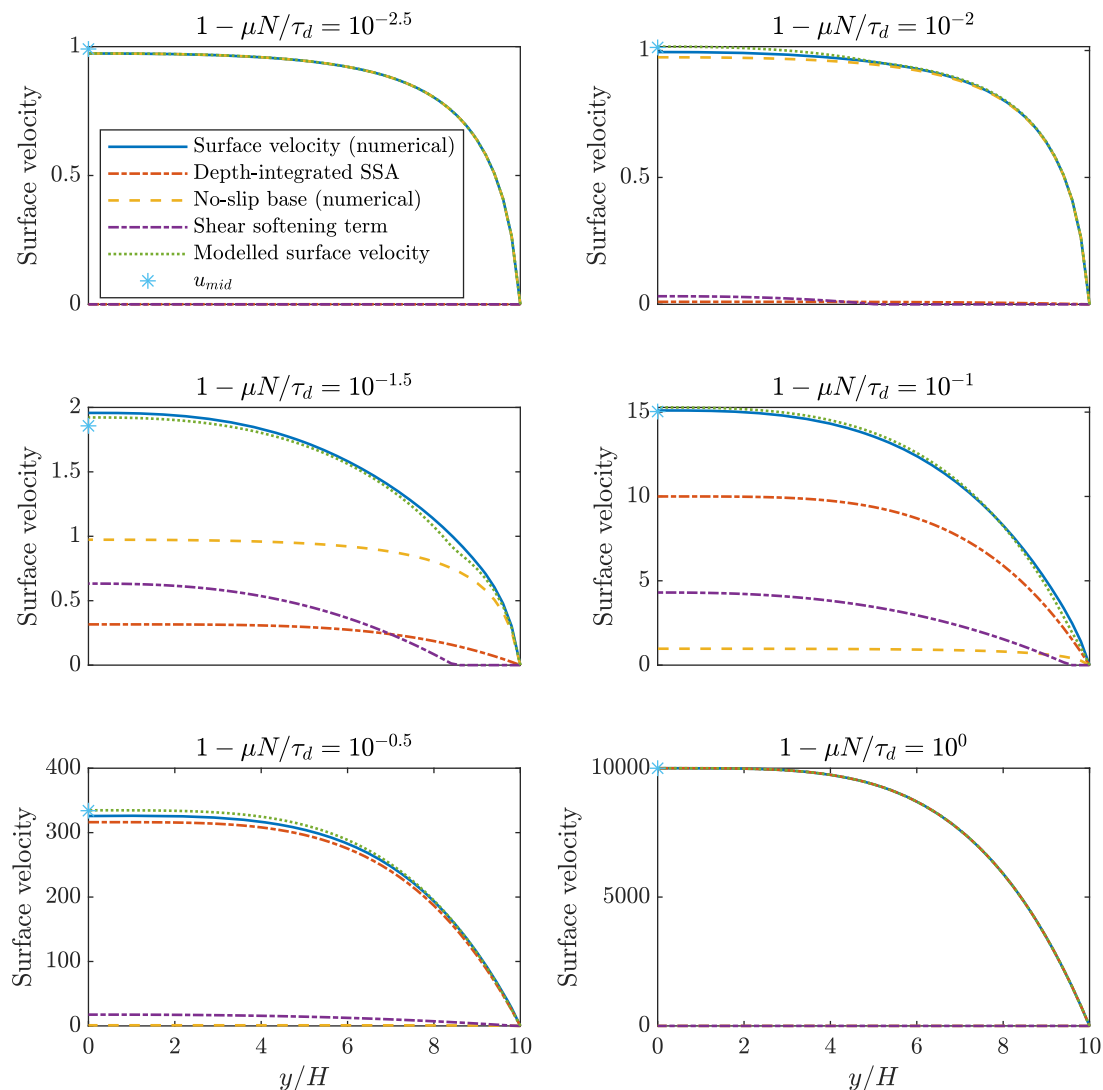
(53)

Figure 8. Numerically calculated profiles of surface velocity for increasing values of $1 - \mu N/\tau_d$, compared to the SSA profile (39), the numerically calculated surface velocity with $u_b = 0$, and the model we propose in (53), taking into account basal shear softening. The velocities are scaled so that the SIA limit is $u_{mid} = 1$.

The predictions of (53) give good agreement with the numerical velocity profiles across the full width of the stream and throughout the full range of bed strengths (Fig. 8).

Simple expressions for surface velocity have been used to estimate ice depth or basal properties (e.g. Li and others, 2012) before recourse to full-Stokes modelling, and our improved estimate of surface velocity could be used to improve the accuracy of such work. However, with uncertainties in ice rheology, bed geometry and basal conditions, it is not possible to simultaneously invert for all unknowns from only a single value, namely maximum surface velocity. In large-scale inversions, the spatial heterogeneity of surface velocity is used as a constraint. In a similar manner, the width of the shear margins and the degree of uniformity across the centre of the stream could potentially provide sufficient constraints to simultaneously constrain ice rheology and basal strength. This could be used, for example, to extend the work of Millstein and others (2022), approximating ice rheology, to grounded ice streams, or to re-examine Minchew and others (2018) beyond the use of the SSA approximation. However, the heterogeneity of real ice stream beds will complicate this kind of analysis.

6. Discussion

We have seen that for ice flowing in a stream over a plastic bed, there are three regimes of behaviour for the ice flow depending on the yield strength of the bed as compared to the driving stress. If the bed exerts very little resistance on the ice, the flow is primarily uniform with depth and resisted by lateral shear from the sidewalls (the SSA regime). If the bed strength is high and the ice cannot slide, vertical shear alone sets the flow field throughout the majority of the ice stream (the SIA regime). Between these limits is a regime where sliding is rapid and lateral stresses are still the primary control on ice speed, but basal drag causes shear of significant enough magnitude to soften the ice, thereby altering the response of the ice stream away from the margnis. We can summarise the effect of this softening through a new term in the expressions for surface velocity (43) and flux (51).

6.1. Ice-stream geometry and ice rheology

We have focused on a rectangular channel geometry which permits several simplifications in our approach. Firstly, we take the depth of the ice to be uniform, which considerably simplifies the integration of the shear profile across the width of the channel. While a cross-stream variation in ice depth would not alter the approach significantly, it would result in more involved analytical calculations. It would also be more complex to apply the traction condition on a sloping boundary, although if this slope is small then to leading order this correction will be linear in the slope

angle. Secondly, in our model setup there is a clear separation between the bed of the stream and the sidewalls, allowing us to cleanly impose different boundary conditions on each surface. While subglacial sediments may be concentrated in the deepest parts of the glacier bed, with sidewalls sloping away from the bed (e.g. Truffer and others, 2001), many ice streams in Antarctica are not confined by topography but found between regions of slower-flowing ice. In fact, one might consider these streams, generated by variations in bed strength, as an extreme example of a very wide channel in which only a narrow central section of the bed has yielded, and any actual sidewalls play a negligible role. Interestingly, this suggests that basal stress-controlled streams could show a different dependence of speed on their width and bed strength than topographically controlled streams – although the controls on the width of the yielded bed are very different from those we consider here. The flow of ice over a flat bed with variable bed strength is considered in Schoof (2004) – the self-consistent determination of the yielded regions of the bed are key to solving for the stress field in this geometry.

We have taken our flow to be uniform in the along-flow direction, which reduces the dimensionality of the problem and removes any extensional stresses. This simplifies the expression for the effective viscosity, as we have assumed either basal shear or lateral shear must dominate in any region of the stream. In fact, at the centre of an ice stream, extensional stresses will dominate if along-flow velocity variations over a distance comparable to the stream width are large relative to maximum flow speeds. Variation on this magnitude is uncommon inland but occurs as ice streams accelerate towards their grounding lines (Mouginot and others, 2017). Including these extensional stresses also introduces longitudinal terms in the force balance. We suggest that a comparison of extensional to lateral stresses in a freely sliding regime is better left to two-dimensional membrane models. Once the dominant horizontal stress relevant to the geometry is identified, basal drag can be introduced either using this work, or the analysis of Schoof and Hindmarsh (2010), who looked at basal drag as a perturbation to extensional flow.

In taking a simple power-law rheology for the ice, we have ignored the complex dependence of ice viscosity on a host of factors, but most pertinently temperature, water content, damage and fabric (grain size and orientation). All of these factors are particularly likely to differ between the bulk of the ice stream and the regions of highest shear, namely in the shear margins and close to the bed (Harrison and others, 1998; Minchew and others, 2018). By considering these as additional mechanisms by which the ice viscosity depends on shear rate, one could attempt to parameterise their effects by using an altered power n in the ice rheology. As such, we have left all the expressions in our results as holding for general n. However, the flow of ice advects heat, damage and water downstream, so the dependence of viscosity on shear rate can be non-local in a way which cannot be fully captured by this steady, uniform model.

We note that all these assumptions in our model setup are common when working with simplified models of ice stream flow. However, it is worth considering, and exploring with more detailed numerical models, whether including basal shear-softening and more accurately capturing flow in this geometry is significant compared to the error introduced by simplifying the ice stream geometry and rheology in the first place.

6.2. Approximations in the analysis

Our mathematical analysis is not of the full-Stokes Eqn. (1) directly, but of an approximation using a linear shapefactor for the vertical shear stress. This approximation can be motivated by the separation of scales between the horizontal and vertical

velocity gradients for wide streams, and the numerical stress fields (Fig. 2) provide reassurance that the approximation is reasonable. Further, the L1L2 model on which it is based is well-tested compared to full-Stokes simulations (Hindmarsh, 2004; Cornford and others, 2013; Robinson and others, 2022). However, this approximation breaks down for narrow streams over strong beds, as can be seen in Figure 5.

Indeed, a question remains as to what happens close to the sidewalls when the bed is not sliding. As discussed in the results, close to the sidewalls the surface velocity and basal stress go to zero across a region of width $\sim H$, which leads to errors in the estimated flux through the ice stream. Numerical analysis of this problem dates back to Nye (1965) and Kozicki and others (1966), but to our knowledge no analytic results exist for the flow of shear-thinning fluids near a corner. The problem is inherently two-dimensional, with significant vertical gradients in horizontal stress that the L1L2 approach is not designed to handle. Further study of these dynamics are certainly interesting from a fluid-dynamical perspective, but beyond the scope of the present paper.

We have calculated the centreline surface velocity in a manner that avoids considering the velocity field above the unyielded region, but our estimate of y_u becomes less accurate as the region widens. Since our estimate of y_u does tend to 0 as $\mu N \to \tau_d$, we have the correct leading order expressions for u_{mid} and Q in this regime. However, the estimate of sliding speed depends directly on y_u and could therefore be improved by more detailed calculation of the dynamics above the unyielded bed (c.f. Haseloff and others, 2019).

6.3. Applicability to other sliding laws

While previous work employing simple expressions for sliding speed and flux through ice streams has mainly centred on flow over a bed of uniform strength, larger scale ice-sheet models more frequently use regularised sliding laws. Here we consider to what extent our results for a constant-strength bed are applicable to sliding laws of the form $u_b = f(\tau_b)$.

If we view our results as a calculation for the basal sliding speed $u_b(\tau_b)$, flux $Q(\tau_b)$, and surface velocity $u_s(\tau_b)$ for a given basal traction, we can look for self-consistent solutions to

$$f(\tau_b) = u_b(\tau_b), \tag{54}$$

effectively approximating the basal traction as its value in the centre of the bed. This allows us to predict the surface velocity and flux as functions of the sliding law and driving stress, which we can again compare to numerically calculated values.

Based on our expression for maximum sliding speed (44), (54) becomes

$$u_b(\tau_b) = 2AH \left[\frac{(\tau_d - \tau_b)^n}{n+1} \frac{W^{n+1}}{H} + \frac{2}{n+2} \left(\frac{n-2}{n-1} \tau_b(\tau_d - \tau_b) \right)^{n/2} \right.$$
$$\left. \times \left(\frac{W}{H} - \frac{\tau_b H}{2(\tau_d - \tau_b)W} \right)^{(n+2)/2} \right] \tag{55}$$

an implicit equation for u_b or τ_b which we cannot directly solve in general, but remains a computationally cheap problem compared to numerical solution of the Stokes equations.

Considering a power-law sliding law of the form
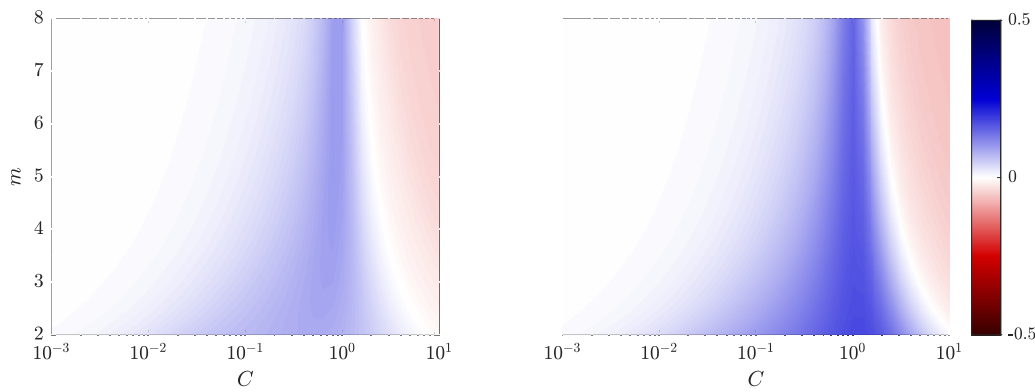
$$\tau_b = C u_b^{1/m}, \tag{56}$$

Figure 9. Fractional error in estimated (left) centreline surface velocity u_{mid} and (right) total flux Q using (54), compared to numerically calculated results with a sliding law of the form (56), for $n = 3$ and $W/H = 8$..
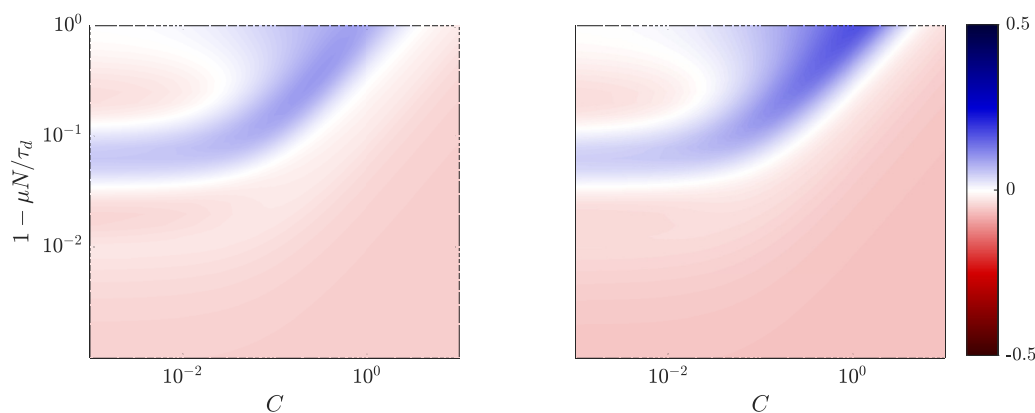

Figure 10. Fractional error in estimated (left) centreline surface velocity u_{mid} and (right) total flux Q using (54), compared to numerically calculated results with a sliding law of the form (58) with $m = 3$, for $n = 3$ and $W/H = 8$..

we see generally reasonable agreement between the numerical and self-consistently calculated values of Q and u_{mid} (Fig. 9). However, the clearest difference between the numerical velocity fields for the plastic bed and power-law sliding is in the surface velocity profiles for very strong beds (large C). This can be attributed to the difference in the shape of the basal velocity profiles as $u_{\mathrm{b}} \to 0$. Over a plastic bed, the margins stop yielding while the centre of the bed continues to slide, the ice above which is resisted primarily by lateral shear – this leads to fairly rounded surface velocity profiles. Over a power-law bed, once $\tau_{\mathrm{b}} \sim \tau_{\mathrm{d}}$, one can rearrange (56) to find a constant sliding speed $u_{\mathrm{b}} = (\tau_{\mathrm{d}}/C)^m$ over the majority of the bed, and without lateral variations in sliding speed, the vertical shear stress dominates the force balance, leading to a correspondingly uniform surface velocity,

$$u_{\mathrm{s}} \approx \frac{\tau_{\mathrm{d}}{}^m}{C} + \frac{2A\tau_{\mathrm{d}}^n H}{n+1}, \qquad (57)$$

with shear margins of order H close to the sidewalls.

We can also look at the impact of mixed sliding laws of the form

$$\tau_{\mathrm{b}} = \mu N + C u_{\mathrm{b}}^{1/m}, \qquad (58)$$

which would correspond to a visco-plastic material at the bed (Iverson, 2010; Warburton and others, 2023). As might be expected, this gives qualitatively similar results to the plastic bed when C is small, and similar results to the power-law bed when C is large. In both regimes the self-consistent method for calculating τ_{b} leads to reasonable agreement with numerically calculated values of Q and u_{mid} (Fig. 10).

The comparisons suggest that our simple expressions for flux and velocity can produce useful results for more general sliding laws, by seeking self-consistent values of basal drag and basal sliding. It again suggests that surface velocity profiles are a key indicator of basal boundary conditions.

Alternatively, we can view the expression for sliding speed as a function of basal shear stress (55) as a mixed boundary condition that an ice stream exerts on its bed. It could be used as a more ice-stream-representative boundary condition in studies of till dynamics, beyond forcing with a constant shear stress or speed.

7. Conclusions

By considering the impact of basal drag on depth-integrated viscosity, we have produced improved expressions for the velocity field in an ice stream flowing over a bed of constant yield strength which capture the transition from the sidewall-resisted regime to the basal shear dominated regime. These more accurate expressions for the surface velocity (43), basal sliding speed (44) and total flux (51) through the stream are simple enough to include in wider models of the interaction of ice streams with their environment, and could also be used to rapidly invert for bed properties given surface observations. While we have focused on a simple geometry and simple ice rheology, these results still provide an improved estimate of ice behaviour under these oft-assumed conditions.

References

Adhikari S and Marshall S (2012) Parameterization of lateral drag in flowline models of glacier dynamics. *Journal of Glaciology* **58**(212), 1119–1132. doi:10.3189/2012JoG12J018

Benn DI, Hulton NR and Mottram RH (2007) 'Calving laws', 'sliding laws' and the stability of tidewater glaciers. *Annals of Glaciology* **46**, 123–130. doi:10.3189/172756407782871161

Blatter H (1995) Velocity and stress fields in grounded glaciers: a simple algorithm for including deviatoric stress gradients. *Journal of Glaciology* **41**(138), 333–344. doi:10.3189/S002214300001621X

Cornford SL and 8 others (2013) Adaptive mesh, finite volume modeling of marine ice sheets. *Journal of Computational Physics* **232**(1), 529–549. doi:10.1016/j.jcp.2012.08.037

Cuffey KM and Paterson WSB (2010) *The Physics of Glaciers*. Amsterdam: Academic Press.

Fowler A (2011) *Mathematical Geoscience*. London: Springer Science & Business Media.

Glen JW (1955) The creep of polycrystalline ice. *Proceedings of the Royal Society A* **228**(1175), 519–538. doi:10.1098/rspa.1955.0066

Goldberg DN and Sergienko OV (2011) Data assimilation using a hybrid ice flow model. *The Cryosphere* **5**, 315–327. doi:10.5194/tc-5-315-2011

Goldsby DL and Kohlstedt DL (2001) Superplastic deformation of ice: experimental observations. *Journal of Geophysical Research: Solid Earth* **106**(B6), 11017–11030. doi:10.1029/2000JB900336

Harrison WD, Echelmeyer KA and Larsen CF (1998) Measurement of temperature in a margin of ice stream B, Antarctica: implications for margin migration and lateral drag. *Journal of Glaciology* **44**(148), 615–624. doi:10.3189/S0022143000002112

Haseloff M, Hewitt IJ and Katz RF (2019) Englacial pore water localizes shear in temperate ice stream margins. *Journal of Geophysical Research: Earth Surface* **124**(11), 2521–2541. doi:10.1029/2019JF005399

Hindmarsh RCA (2004) A numerical comparison of approximations to the Stokes equations used in ice sheet and glacier modeling. *Journal of Geophysical Research: Earth Surface* **109**(F1), F01012. doi:10.1029/2003JF000065

Hunter P, Meyer C, Minchew B, Haseloff M and Rempel A (2021) Thermal controls on ice stream shear margins. *Journal of Glaciology* **67**(263), 435–449. doi:10.1017/jog.2020.118

Iverson NR (2010) Shear resistance and continuity of subglacial till: hydrology rules. *Journal of Glaciology* **56**(200), 1104–1114. doi:10.3189/002214311796406220

Joughin I, Smith BE and Schoof CG (2019) Regularized Coulomb friction laws for ice sheet sliding: application to Pine Island Glacier, Antarctica. *Geophysical Research Letters* **46**(9), 4764–4771. doi:10.1029/2019GL082526

Kamb B (2001) Basal zone of the West Antarctic ice streams and its role in lubrication of their rapid motion. In Alley RB and Bindschadler RA (eds), *The West Antarctic Ice Sheet: Behavior and Environment*, American Geophysical Union (AGU), pp. 157–199.

Kamb B and Echelmeyer KA (1986) Stress-gradient coupling in glacier flow: I. longitudinal averaging of the influence of ice thickness and surface slope. *Journal of Glaciology* **32**(111), 267–284. doi:10.3189/S0022143000015604

Kozicki W, Chou C and Tiu C (1966) Non-Newtonian flow in ducts of arbitrary cross-sectional shape. *Chemical Engineering Science* **21**(8), 665–679. doi:10.1016/0009-2509(66)80016-7

Li H, Ng F, Li Z, Qin D and Cheng G (2012) An extended 'perfect-plasticity' method for estimating ice thickness along the flow line of mountain glaciers. *Journal of Geophysical Research: Earth Surface* **117**(F1), F01020. doi:10.1029/2011JF002104

MacAyeal DR (1989) Large-scale ice flow over a viscous basal sediment: theory and application to Ice Stream B, Antarctica. *Journal of Geophysical Research: Solid Earth* **94**(B4), 4071–4087. doi:10.1029/JB094iB04p04071

Mann LE, Robel AA and Meyer CR (2021) Synchronization of Heinrich and Dansgaard-Oeschger events through ice-ocean interactions. *Paleoceanography and Paleoclimatology* **36**(11), e2021PA004334. doi:10.1029/2021PA004334

Meyer CR and Minchew BM (2018) Temperate ice in the shear margins of the Antarctic ice sheet: controlling processes and preliminary locations. *Earth and Planetary Science Letters* **498**, 17–26. doi:10.1016/j.epsl.2018.06.028

Millstein JD, Minchew BM and Pegler SS (2022) Ice viscosity is more sensitive to stress than commonly assumed. *Communications Earth & Environment* **3**(1), 57. doi:10.1038/s43247-022-00385-x

Minchew B and 7 others (2016) Plastic bed beneath Hofsjökull ice cap, central Iceland, and the sensitivity of ice flow to surface meltwater flux. *Journal of Glaciology* **62**(231), 147–158. doi:10.1017/jog.2016.26

Minchew BM and Meyer CR (2020) Dilation of subglacial sediment governs incipient surge motion in glaciers with deformable beds. *Proceedings of the Royal Society A* **476**(2238), 20200033. doi:10.1098/rspa.2020.0033

Minchew BM, Simons M, Riel B and Milillo P (2017) Tidally induced variations in vertical and horizontal motion on Rutford Ice Stream, West Antarctica, inferred from remotely sensed observations. *Journal of Geophysical Research: Earth Surface* **122**(1), 167–190. doi:10.1002/2016JF003971

Minchew BM, Meyer CR, Robel AA, Gudmundsson GH and Simons M (2018) Processes controlling the downstream evolution of ice rheology in glacier shear margins: case study on Rutford Ice Stream, West Antarctica. *Journal of Glaciology* **64**(246), 583–594. doi:10.1017/jog.2018.47

Morland LW (1987) Unconfined ice-shelf flow. In Van der Veen CJ and Oerlemans J (eds), *Dynamics of the West Antarctic Ice Sheet*, Dordrecht: Springer Netherlands, pp. 99–116.

Mouginot J, Rignot E, Scheuchl B and Millan R (2017) Comprehensive annual ice sheet velocity mapping using Landsat-8, Sentinel-1, and RADARSAT-2 data. *Remote Sensing* **9**(4), 364. doi:10.3390/rs9040364

Nye JF (1965) The flow of a glacier in a channel of rectangular, elliptic or parabolic cross-section. *Journal of Glaciology* **5**(41), 661–690. doi:10.3189/S0022143000018670

Pattyn F (2003) A new three-dimensional higher-order thermomechanical ice sheet model: basic sensitivity, ice stream development, and ice flow across subglacial lakes. *Journal of Geophysical Research: Solid Earth* **108**(B8), 2382. doi:10.1029/2002JB002329

Raymond C (1996) Shear margins in glaciers and ice sheets. *Journal of Glaciology* **42**(140), 90–102. doi:10.3189/S0022143000030550

Robinson A, Goldberg D and Lipscomb WH (2022) A comparison of the stability and performance of depth-integrated ice-dynamics solvers. *The Cryosphere* **16**(2), 689–709. doi:10.5194/tc-16-689-2022

Rosier SHR, Gudmundsson GH and Green JAM (2015) Temporal variations in the flow of a large Antarctic ice stream controlled by tidally induced changes in the subglacial water system. *The Cryosphere* **9**(4), 1649–1661. doi:10.5194/tc-9-1649-2015

Schoof C (2004) On the mechanics of ice-stream shear margins. *Journal of Glaciology* **50**(169), 208–218. doi:10.3189/172756504781830024

Schoof C (2006) Variational methods for glacier flow over plastic till. *Journal of Fluid Mechanics* **555**, 299–320. doi:10.1017/S0022112006009104

Schoof C and Hindmarsh RCA (2010) Thin-film flows with wall slip: an asymptotic analysis of higher order glacier flow models. *The Quarterly Journal of Mechanics and Applied Mathematics* **63**(1), 73–114. doi:10.1093/qjmam/hbp025

Truffer M, Echelmeyer KA and Harrison WD (2001) Implications of till deformation on glacier dynamics. *Journal of Glaciology* **47**(156), 123–134. doi:10.3189/172756501781832449

Warburton KLP, Hewitt DR and Neufeld JA (2023) Shear dilation of subglacial till results in time-dependent sliding laws. *Proceedings of the Royal Society A* **479**(2269), 20220536. doi:10.1098/rspa.2022.0536

Weertman J (1957) On the sliding of glaciers. *Journal of Glaciology* **3**(21), 33–38. doi:10.3189/S0022143000024709